

Effect of the Synthetic Method and Support Porosity on the Structure and Performance of Silica-Supported CuBr/Pyridylmethanimine Atom Transfer Radical Polymerization Catalysts. I. Catalyst Preparation and Characterization

JOSEPH V. NGUYEN, CHRISTOPHER W. JONES

School of Chemical and Biomolecular Engineering, Georgia Institute of Technology, 311 Ferst Drive, Atlanta, Georgia 30332

Received 2 September 2003; accepted 21 November 2003

ABSTRACT: Silica-supported CuBr/pyridylmethanimine (PMI) complexes that facilitate the atom transfer radical polymerization of methyl methacrylate have been prepared and characterized. Four different synthetic routes, including multistep-grafting (M1), two-step-grafting (M2), one-pot (M3), and preassembled-complex (M4) methods, have been evaluated on three different silica supports (mesoporous SBA15 with 48- and 100-Å pores and nonporous Cab-O-Sil EH5). The resulting solids have been characterized by a battery of techniques, including thermogravimetric analysis/differential scanning calorimetry, FT-Raman spectroscopy, ^{13}C and ^{29}Si magic-angle-spinning and cross-polarity/magic-angle-spinning spectroscopy, low-temperature nitrogen physisorption, and elemental analysis. The combination of elemental analysis and spectroscopic results has indicated that a variety of different surface species likely exist for most catalysts, including copper species that are both monocoordinated and biscoordinated by PMI ligands, and PMI-free copper bromide species interacting with the silica surface. M4 appears to give a material that has the smallest amount of the uncomplexed ligand (by FT-Raman spectroscopy) and is, therefore, the most homogeneous. After M4, the metallation efficiency decreases in the order $\text{M2} \geq \text{M3} > \text{M1}$, with M1 giving a material with a highly heterogeneous surface composition. The ligand loading on all the catalysts has been determined to be approximately 1 mmol/g of SiO_2 , with Cab-O-Sil-supported materials giving much higher ligand densities because of its lower surface area. © 2004 Wiley Periodicals, Inc. *J Polym Sci Part A: Polym Chem* 42: 1367–1383, 2004

Keywords: atom transfer radical polymerization (ATRP); catalysis; silicas

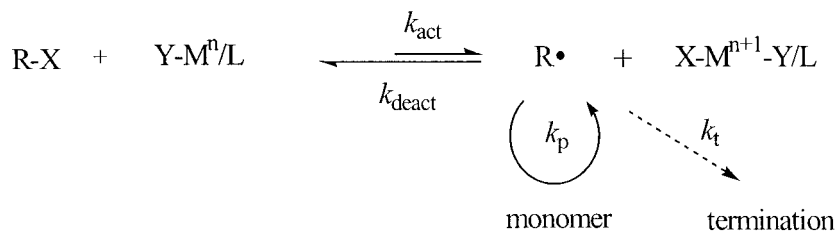
INTRODUCTION

Atom transfer radical polymerization (ATRP) has been the subject of intense research since 1995, when the technique was first reported by Wang

and Matyjaszewski^{1–3} and Sawamoto et al.⁴ independently. In addition to its ability to control the architecture of the final polymer product [i.e., the molecular weight, polydispersity index (weight-average molecular weight/number-average molecular weight), and end functionality], ATRP is an attractive methodology because the process can polymerize a wide range of monomers, requires mild reaction conditions, and is tolerant of impurities.⁵ ATRP is based on a metal/ligand

Correspondence to: C. W. Jones (E-mail: cjones@chbe.gatech.edu)

Journal of Polymer Science: Part A: Polymer Chemistry, Vol. 42, 1367–1383 (2004)
© 2004 Wiley Periodicals, Inc.



Scheme 1

complex that has a high affinity toward halogen atoms and has two accessible oxidation states separated by one electron. A dynamic equilibrium between these redox states is strongly shifted toward deactivation ($k_{\text{act}} \ll k_{\text{deact}}$), and so the overall radical concentration is kept low; this allows for controlled polymerizations (see Scheme 1). Despite the bimolecular radical coupling or termination reactions that occur in a small percentage of the total growing polymer chains, well-behaved ATRP, with limited termination, affords polymers with narrow molecular weight distributions (i.e., polydispersity index ~ 1.2 or better). Because of the ability of the methodology to allow for excellent control over radical polymerizations, investigations of ATRP have skyrocketed, now including studies concerning ATRP initiated from surfaces,^{6,7} in miniemulsions,^{8–11} and in combinatorial investigations.¹²

ATRP typically uses one metal/ligand complex to mediate one growing polymer chain to achieve reasonable reaction rates and good polymerization control.¹³ Therefore, a high concentration of metal is needed to mediate the polymerization, and as a result, the final polymer is colored because of the residual metal. Many postpolymerization purification workup methods have been devised to remove the soluble catalyst from the polymer, but these methods tend to be expensive or wasteful.^{14–20} In some cases, the metal complex is often decomposed, and the metal is discarded.^{14,16,17,19,20} Immobilizing the catalyst on a solid support has been an attractive potential solution. The immobilization facilitates catalyst recovery, and with the proper method used to regenerate the metal/ligand complex, the catalyst can potentially be recycled.

There are many examples in the literature involving the immobilization of an ATRP metal/ligand complex on various supports. Matyjaszewski and coworkers,^{21–25} Haddleton and coworkers,^{26,27} Brittain and coworkers,^{28,29} Zhu and coworkers,^{30–36} and others³⁷ have reported immo-

bilized ATRP catalysts. However, for a number of reasons, these surface-mediated polymerization methods allow for limited control over the polymerization.

Potential transport limitations associated with heterogeneous catalysis are well known. When dealing with high-molecular-weight polymer species in and around solid supports, potential diffusion limitations can be greatly exacerbated. Poor polymerization control in earlier investigations was generally attributed to a poor deactivation of the growing polymer chain.²³ The deactivation step is affected by the mobility of the immobilized catalyst on the support and the rate of diffusion of the polymer chains in the reaction mixture. For this reason, catalysts that have highly accessible complexes, such as those that use flexible supports²⁹ or long surface-complex linkages,³⁴ are among the most effective. If the growing radical terminated chain does not encounter a high-oxidation-state metal complex and become deactivated readily enough, the propagation of the polymer chain becomes uncontrolled. Therefore, the size, porosity, and solubility of the catalyst particle ultimately affect the polymerization. Most recently, Matyjaszewski and coworkers^{22,23} introduced a mixed heterogeneous/homogeneous catalyst system to gain better control over the polymerization. They found that through the addition of a small amount of a soluble deactivator complex, $\text{CuBr}_2/\text{tris}(2\text{-(dimethylamino)ethyl})\text{-amine}$ ($\text{CuBr}_2/\text{Me}_6\text{TREN}$), the deactivation process was facilitated and the polymerization proceeded in a controlled manner. The soluble deactivator has been proposed to act as a shuttling agent, transferring the halogen to the growing polymer chain and thereby deactivating the chain and keeping the overall radical concentration low. Even though only a small percentage of the soluble deactivator is introduced into the polymerization, the soluble copper catalyst is eventually left in the polymer product. Although the use of this soluble deactivator appears to be the best solution

proposed to date for producing a (mostly) recoverable catalyst with good control, alternate solid catalyst designs may still yield a well-behaved catalyst that is entirely heterogeneous.

As mentioned previously, there have been various degrees of success with polymerizations with heterogeneous ATRP catalyst systems. Matyjaszewski and coworkers^{22–25} immobilized copper(I) bromide (CuBr)/bipyridine complex-soluble CuBr₂/Me₆TREN system and Haddleton et al.'s²⁶ and Brittain et al.'s^{28,29} immobilized CuBr/pyridylmethanimine (PMI) complexes are the most well studied heterogeneous systems that possess some degree of control in radical polymerizations. In the homogeneous catalyst systems, the activating species in both cases are believed to contain two chelating ligands coordinated tetrahedrally to one CuBr.^{38–41} Ideally, the immobilized complex should have a structure similar to that of the homogeneous system.

Two general synthetic schemes have been used to immobilize Cu ATRP catalysts on inorganic or organic supports. In the first method, the complex is built stepwise on the solid with a grafting approach.^{22,23,26,28,29,32} This can lead to a highly heterogeneous surface with multiple types of copper sites formed with various reactivities. As an alternative, the complex can be preassembled homogeneously, and this homogeneous complex can be immobilized on the solid. Although this approach has not been routinely used in ATRP catalyst design, supported copper complexes have been prepared with this methodology for other purposes.^{42–44} Both of these methodologies and hybrids of the two approaches are systematically explored here.

In addition to designing the molecular active site, one also has to carefully control the properties of the support. Primarily, organic polymers^{22–26,28,29,32,35} and silica^{21,23,26,27,30,31,33–37} have been used as supports because of their low cost and ease of handling. In the case of porous inorganic polymers such as silica, the exact nature of the porosity can have a strong impact on the catalytic properties, especially when transport plays an important role. Because the accessibility of the growing chains to the deactivating surface-bound metal complexes can be critical in ATRP,^{21,23} understanding the role of porosity is extremely important. Here we report a systematic study of the role of the synthetic methodology and support structure in the ATRP of methyl methacrylate (MMA) with silica-supported CuBr/PMI catalysts.

In the first part of this work, we investigate four different synthetic protocols for the immobilization of CuBr/PMI⁴⁵ complexes on various silica supports and characterize the resulting solids. In second part of this series, we will report the performance of these catalysts in the polymerization of MMA.⁴⁶

EXPERIMENTAL

Chemicals

Methylene chloride-*d*₂ (CD₂Cl₂; Cambridge Isotope Laboratories, Inc.; 99.8%), chloroform-*d* (CDCl₃; Cambridge Isotope Laboratories, Inc.; 99.8%), and propylamine (Acros; >99%) were dried over 4-Å molecular sieves and stored under nitrogen. CuBr (Acros; 98%) was purified via stirring in glacial acetic acid for 5 h, washed with absolute ethanol and anhydrous diethyl ether, dried *in vacuo* for 12 h at room temperature, and stored under nitrogen. Anhydrous methanol (MeOH; Alfa Aesar; >99%), 3-aminopropyltrimethoxysilane (APTMS; Aldrich; 97%), and 2-pyridinecarboxaldehyde (PCA; Aldrich; 99%) were used as received and stored under nitrogen. Cab-O-Sil EH5 (Cabot) was dried *in vacuo* for 12 h at room temperature and stored under nitrogen. Poly(ethylene glycol)-*block*-poly(propylene glycol)-*block*-poly(ethylene glycol) (EO-PO-EO; Aldrich), hydrochloric acid (HCl; JT-Baker), tetraethyl orthosilicate (TEOS; Acros; 98%), and 1,3,5-trimethylbenzene (TMB; Aldrich; 97%) were used as received. Hexanes (Aldrich; >99%) and methylene chloride (CH₂Cl₂; Aldrich; >99%) were dried and deoxygenated with a purification system and were stored under nitrogen in a glove box.⁴⁷

Characterization

Thermogravimetric analysis (TGA) was carried out with a Netzsch STA 409 PC Luxx simultaneous thermal analyzer (TGA/differential scanning calorimetry) with heating to 1000 °C at 20 K/min. The silica pore diameters and surface areas were determined with nitrogen physisorption data obtained with a Micromeritics ASAP 2000 system. The samples were pretreated at 90 °C for 1 h and at 150 °C overnight *in vacuo*. The surface areas were analyzed by the Brunauer–Emmett–Teller (BET) method, and the pore size distribution was determined with the Barrett–Joyner–

Halenda (BJH) method applied to the adsorption branch of the isotherm.⁴⁸ X-ray powder diffraction patterns were recorded with Cu K α radiation on a Scintag X1 powder diffractometer. FT-Raman spectroscopy was performed with a Bruker IFS 66 v/S equipped with dual Fourier transform infrared (FTIR) and Fourier transform/Raman (FT-Raman) benches and a CaF₂ beam splitter. ¹H and ¹³C solution NMR measurements were performed with a Mercury Vx 300-MHz instrument with CD₂Cl₂ or CDCl₃ as a solvent. Solid-state ¹³C and ²⁹Si cross-polarity/magic-angle-spinning (CP-MAS) NMR spectra were collected on Bruker DSX 300- and 400-MHz instruments, respectively. Typical ¹³C CP-MAS parameters were 10,000 scans, a 90° pulse length of 4 μ s, and a delay of 4 s between scans. Typical ²⁹Si CP-MAS parameters were 2000 scans, a 90° pulse length of 5 μ s, and a delay of 10 s between scans. Copper and silicon elemental analysis (EA) was performed by Galbraith Laboratories, Inc. (Knoxville, TN) or Chemisar Laboratories (Guelph, Canada) with inductively coupled plasma atomic emission spectroscopy (AES). Carbon, hydrogen, and nitrogen contents were determined via CHN analysis by Galbraith Laboratories or Chemisar Laboratories.

Synthesis of [3-(Trimethoxysilyl)-propyl]-2-pyridylmethanimine (PMITMS)

To a 100-mL, round-bottom flask were added 5.54 g of APTMS (0.031 mol), 3.64 g of PCA (0.034 mol), and 30 mL of anhydrous MeOH. The reaction solution was stirred at 75 °C for 24 h under argon. The product was isolated by the removal of the light volatiles (MeOH and PCA) by vacuum distillation and stored under dry nitrogen in a glove box to yield a dark brown, viscous oil (C₁₂H₂₀N₂O₃Si; 90% yield and 99% purity).

¹H NMR (CD₂Cl₂, δ): 0.69 (t, 2H, —SiCH₂—), 1.81 (m, 2H, —SiCH₂CH₂—), 3.55 [s, 9H, (—Si—OCH₃)₃], 3.65 (t, 2H, —SiCH₂CH₂CH₂—), 7.32 (t, 1H, —CCHCHCHCHN—), 7.75 (t, 1H, —CCHCHCHCHN—), 8.00 (d, 1H, —CCHCHCHCHN—), 8.35 (s, 1H, —CH₂NCH—), 8.61 (d, 1H, —CCHCHCHCHN—). ¹³C NMR (CDCl₃, δ): 8.67 (—SiCH₂—), 24.47 (—SiCH₂CH₂—), 50.55 (—SiCH₂CH₂CH₂N—), 64.22 [—Si—(OCH₃)₃], 121.33 (—CCHCHCHCHN—), 124.76 (—CCHCHCHCHN—), 136.62 (—CCHCHCHCHN—), 149.50 (—CCHCHCHCHN—), 154.71 (—CCHCHCHCHN—), 162.04 (—CH₂CH₂N=CH—).

Material Syntheses

SBA15 (48-Å Pores)

Mesoporous silica SBA15 was synthesized with the triblock EO-PO-EO nonionic surfactant as the structure-directing agent.^{49,50} In a typical preparation, 12.43 g of EO-PO-EO, 273.92 g of deionized H₂O, and 86.60 g of 38% aqueous HCl were stirred at room temperature until the triblock copolymer completely dissolved. Then, 27.05 g of TEOS was added to the solution, and the solution was stirred for 5 min. The mixture was distributed into 10 Parr Teflon-line autoclaves and agitated at 50 °C for 20 h. The solid product was recovered by filtration, washed with deionized H₂O extensively, and air-dried at 50 °C overnight. Calcination was carried out, the temperature slowly increasing from room temperature to 200 °C at 1.2 K/min, under a nitrogen-enriched atmosphere. The temperature was held at 200 °C for 1 h and then slowly increased to 500 °C at 2 K/min under an oxygen-enriched atmosphere. The temperature was held at 500 °C for 6 h. The solid product was dried *in vacuo* for 12 h and stored under dry nitrogen in a glove box; approximately 8 g of the solid was yielded.

SBA15 (100-Å Pores)

Large-pore SBA15 was synthesized similarly to the 48-Å material, except that TMB was used as a swelling cosolvent. In a typical preparation, 12.00 g of EO-PO-EO, 317.77 g of deionized H₂O, 1.50 g of TMB, and 86.60 g of 38% aqueous HCl were stirred at room temperature until the triblock copolymer completely dissolved. Then, 25.63 g of TEOS was added to the solution, and the solution was stirred for 5 min. The mixture was distributed into 10 Parr Teflon-line autoclaves and agitated at 35 °C for 20 h and was then aged at 100 °C without stirring for 24 h. The solid product was recovered by filtration, washed with deionized H₂O extensively, and air-dried at 50 °C overnight. Calcination was carried out under the same conditions described for the 48-Å-pore material. The solid product was dried *in vacuo* for 12 h and stored under dry nitrogen in a glove box; approximately 8 g of the solid was yield.

Syntheses of the CuBr/PMI-Immobilized Catalysts

All the catalyst syntheses described were prepared, recovered, and washed under dry nitrogen in a glove box. Schlenk techniques were used for

manipulating the reaction mixtures outside the nitrogen glove box. All solvents used in the syntheses of these materials were anhydrous and deoxygenated.

Preparation of the SBA15(48 Å)-CuBr/PMI-Immobilized Catalyst

Method 1 (M1). Multistep-Grafting Approach: SBA15(48)-CuBr/PMI-M1

Preparation of the Amine-Functionalized Silica Surface: SBA15(48)-NH₂-M1. To a 250-mL, round-bottom flask, 2.00 g of APTMS was added to a slurry of 3.00 g of SBA15 (48-Å pores) in 100 mL of toluene. The reaction mixture was stirred at 110 °C for 48 h under argon. The solid product was recovered and washed, once with 100 mL of toluene, once with 100 mL of hexane, and once with 100 mL of dichloromethane. The solid product was dried *in vacuo* at room temperature for 12 h and stored under dry nitrogen in a glove box, yielding a white powder containing 1.36 mmol of —NH₂/g of solid according to TGA.

Preparation of the SBA15(48 Å)-PMI-Functionalized Surface: SBA15(48)-PMI-M1. To a 250-mL, round-bottom flask, 1.09 g of PCA (10.2 mmol) was added to a slurry of 2.50 g of SBA15(48)-NH₂-M1 (3.4 mmol of amine) in 100 mL of MeOH. The reaction mixture was stirred at 75 °C for 24 h under argon. The solid product was recovered and washed, once with 100 mL of toluene, once with 100 mL of hexane, and once with 100 mL of dichloromethane. The solid product was dried *in vacuo* at room temperature for 12 h and stored under dry nitrogen in a glove box, yielding a yellowish-white powder containing 1.13 mmol of PMI/g of solid according to TGA.

Metallation of SBA15(48 Å)-PMI with CuBr: SBA15(48)-CuBr/PMI-M1. To a 100-mL, round-bottom flask, 0.16 g of CuBr (1.13 mmol) was added to a slurry of 2.00 g of SBA15(48)-PMI-M1 (2.26 mmol of ligand) in 50 mL of toluene. The reaction mixture was stirred at 110 °C for 24 h under argon. The solid product was recovered and washed, once with 100 mL of toluene, once with 100 mL of hexane, and once with 100 mL of dichloromethane. The dark reddish-brown powder was dried *in vacuo* at room temperature for 12 h and stored under dry nitrogen in a glove box. CHN, Si, and Cu analyses showed 1.07 mmol of

PMI/g of catalyst and 0.48 mmol of Cu/g of catalyst.

Method 2 (M2). Two-Step Approach: SBA15(48)-CuBr/PMI-M2

Preparation of the SBA15(48 Å)-PMI-Functionalized Surface: SBA15(48)-PMI-M2. To a 250-mL, round-bottom flask, 1.50 g of PMITMS was added to a slurry of 3.00 g of SBA15 (48-Å pores) in 100 mL of toluene. The reaction mixture was stirred at 110 °C for 48 h under argon. The solid product was recovered and washed, once with 100 mL of toluene, once with 100 mL of hexane, and once with 100 mL of dichloromethane. The solid product was dried *in vacuo* at room temperature for 12 h and stored under dry nitrogen in a glove box, yielding a yellow powder containing 1.04 mmol of PMI/g of solid according to TGA.

Metallation of SBA15(48 Å)-PMI with CuBr: SBA15(48)-CuBr/PMI-M2. To a 100-mL, round-bottom flask, 0.15 g of CuBr (1.04 mmol) was added to a slurry of 2.00 g of SBA15(48)-PMI-M2 (2.08 mmol of ligand) in 50 mL of toluene. The reaction mixture was stirred at 110 °C for 24 h under argon. The solid product was recovered and washed, once with 100 mL of toluene, once with 100 mL of hexane, and once with 100 mL of dichloromethane. The dark reddish-brown powder was dried *in vacuo* at room temperature for 12 h and stored under dry nitrogen in a glove box. CHN, Si, and Cu analyses showed 1.09 mmol of PMI/g of catalyst and 0.51 mmol of Cu/g of catalyst.

Method 3 (M3). One-Pot Approach: SBA15(48)-CuBr/PMI-M3

To a 250-mL, round-bottom flask, 1.00 g of PMITMS (3.73 mmol) was added to a slurry of 0.27 g of CuBr (1.86 mmol) and 2.00 g of SBA15 (48-Å pores) in 100 mL of toluene. The reaction mixture was stirred at 110 °C for 48 h under argon. The solid product was recovered and washed, once with 100 mL of toluene, once with 100 mL of hexane, and once with 100 mL of dichloromethane. The dark reddish-brown powder was dried *in vacuo* at room temperature for 12 h and stored under dry nitrogen in a glove box. CHN, Si, and Cu analyses showed 1.02 mmol of PMI/g of catalyst and 0.42 mmol of Cu/g of catalyst.

Table 1. CHN, Si, and Cu Elemental Analysis (EA)

Entry	Materials	Carbon (%)	Hydrogen (%)	Nitrogen (%)	Silicon (%)	Copper (%)
1	SBA(48)-CuBr/PMI-M1	10.84	1.86	2.40	34.63	1.80
2	SBA(48)-CuBr/PMI-M2	14.26	2.06	2.72	32.79	2.59
3	SBA(48)-CuBr/PMI-M3	15.22	2.06	2.65	32.55	2.80
4	SBA(48)-CuBr/PMI-M4	15.10	1.89	2.75	31.63	2.05
5	SBA(100)-CuBr/PMI-M1	15.30	2.47	3.00	28.87	3.59
6	SBA(100)-CuBr/PMI-M2	12.31	1.74	2.91	29.70	2.66
7	SBA(100)-CuBr/PMI-M3	13.72	1.64	3.23	29.17	3.13
8	SBA(100)-CuBr/PMI-M4	15.67	2.76	3.48	36.60	3.34
9	Cab-O-Sil-CuBr/PMI-M1	10.38	1.13	2.47	36.71	2.69
10	Cab-O-Sil-CuBr/PMI-M2	10.77	2.04	2.44	33.60	2.14
11	Cab-O-Sil-CuBr/PMI-M3	13.14	1.41	3.18	27.90	3.89
12	Cab-O-Sil-CuBr/PMI-M4	13.83	1.34	3.30	33.56	3.06

Method 4 (M4). Preassembled-Complex Approach: SBA15(48)-CuBr/PMI-M4

To a 250-mL, two-necked, round-bottom flask, a solution of 1.00 g of PMITMS (3.73 mmol) and 5 mL of toluene was slowly added to a stirring mixture of 0.27 g of CuBr (1.86 mmol) in 100 mL of toluene. The resulting light brown mixture was then stirred at 70 °C for 30 min under argon or until the reaction mixture appeared to be a dark reddish-brown homogeneous solution. Under positive argon pressure, 2.00 g of SBA15 (48-Å pores) was added to the reaction mixture through the flask's second neck. Then, the reaction mixture was stirred at 110 °C for 48 h. The solid product was recovered and washed, once with 100 mL of toluene, once with 100 mL of hexane, and once with 100 mL of dichloromethane. The dark reddish-brown powder was dried *in vacuo* at room temperature for 12 h and stored under dry nitrogen in a glove box. CHN, Si, and Cu analyses showed 1.07 mmol of PMI/g of catalyst and 0.48 mmol of Cu/g of catalyst.

Preparation of SBA15(100 Å) and Cab-O-Sil EH5: CuBr/PMI-Immobilized Catalyst (M1-M4)

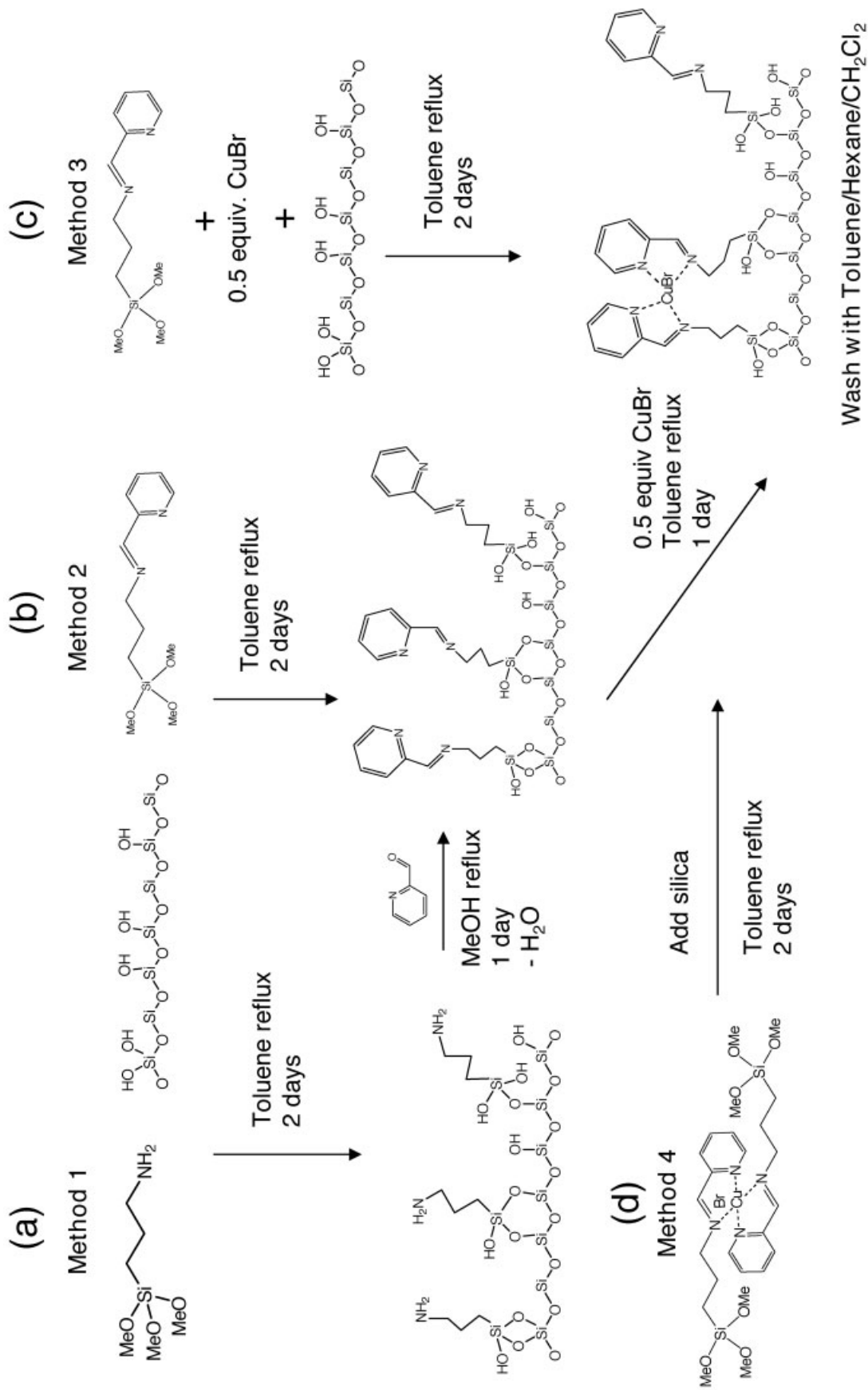
In a manner similar to the aforementioned methods for SBA15 (48-Å pores), a supported CuBr/PMI complex was immobilized on larger pore SBA15 (100-Å pores) and nonporous Cab-O-Sil EH5 silica supports for all methods (M1-M4). All the immobilized catalysts were recovered, washed, and stored under the same conditions. CHN, Si, and Cu analyses are summarized in Table 1.

RESULTS AND DISCUSSION

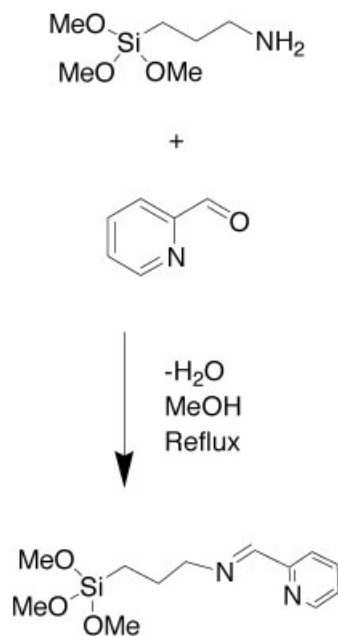
Four different methods of immobilizing CuBr/PMI complexes on silica have been used. Each subsequent method has been designed to potentially reduce the heterogeneity of the surface sites in the solid. M1, shown in Scheme 2(a), is the multistep approach outlined previously by Haddleton et al.²⁶ and Brittain and coworkers.^{28,29} The last three methods incorporate the use of the PMITMS immobilizable ligand. Like M1, the metallation step for M2, the two-step approach, occurs after the ligand has been covalently grafted to the silica surface [Scheme 2(b)]. In M3 and M4, the CuBr/PMI complex is formed *in situ*; these methods are called the one-pot [Scheme 2(c)] and preassembled-complex [Scheme 2(d)] approaches, respectively. Each synthetic approach was applied to mesoporous SBA15 with 48- and 100-Å pores and the nonporous, fumed silica Cab-O-Sil EH5.

Synthesis and Spectroscopic Studies of PMITMS

The immobilizable PMI ligand PMITMS was synthesized homogeneously with methods similar to the approach used for homogeneous and supported PMI ligand.^{26,28,29,40,41} Care was taken to ensure that the PMI ligand was pure because it was straightforward to purify the ligand before its addition to the support, unlike in some previous studies of supported Cu ATRP catalysts.³³ An excess of PCA was added to APTMS, with the excess PCA removed via careful vacuum distillation after the reaction (Scheme 3). The disappearance of the aldehyde proton and amine protons, as



Scheme 2



Scheme 3

well as the appearance of the imine proton, was monitored by ^1H NMR. The quantitative conversion of the aldehyde group to the imine was

achieved, and the immobilizable ligand was recovered free of any residual starting materials that could lead to unselective binding sites on the surface (the ^1H NMR spectrum is shown in Fig. 1).

The synthesis and immobilization of PMITMS were followed by FT-Raman spectroscopy (Fig. 2), and the characteristic Raman shifts are summarized in Table 2.⁵¹ In Figure 2(a), the $\nu(\text{N—H})$ and $\nu(\text{aliphatic C—H})$ vibrations for APTMS appear at 3313 and 2800–2900 cm^{-1} , respectively. Unfortunately, the vibrations due to $\nu(\text{Si—OMe})$ at 1190–1100 and 850–800 cm^{-1} were not strong enough to be detected conclusively. Figure 2(b) shows the FT-Raman spectrum of PCA; the $\nu(\text{aromatic C—H})$, $\nu(\text{CHO})$, $\nu(\text{pyridyl ring})$, and $\nu(\text{in-plane CH})$ vibrations appear at 3056, 1708, 1585, and 993 cm^{-1} , respectively. The FT-Raman spectrum of PMITMS resulting from the reaction of APTMS and PCA is shown in Figure 2(c). The two spectra [Fig. 2(a,b)] can be superimposed, and the disappearance of $\nu(\text{N—H})$ and $\nu(\text{CHO})$, along with the appearance of $\nu(\text{imine})$ at 1650 cm^{-1} , has been noted. The metal complex was subsequently formed when 2 equiv of PMITMS and 1 equiv of

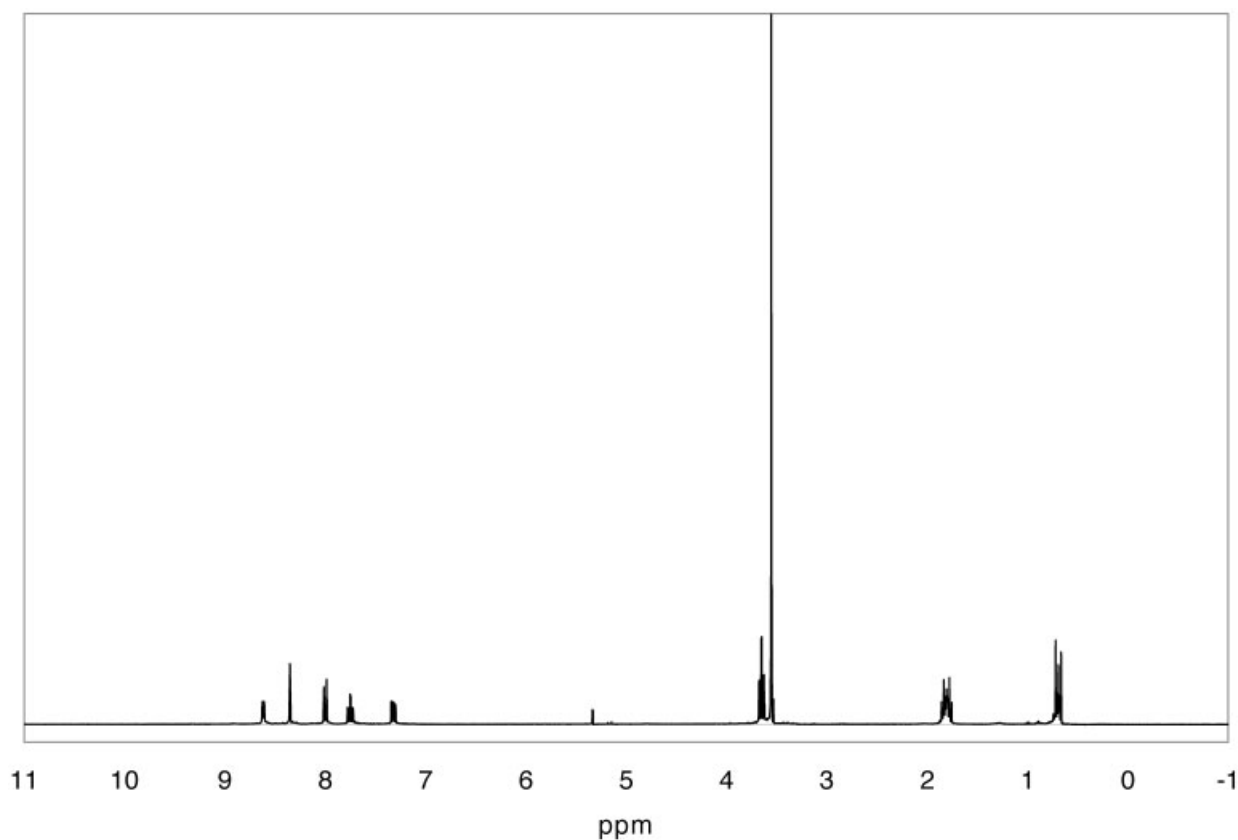


Figure 1. ^1H NMR spectrum of PMITMS in CD_2Cl_2 .

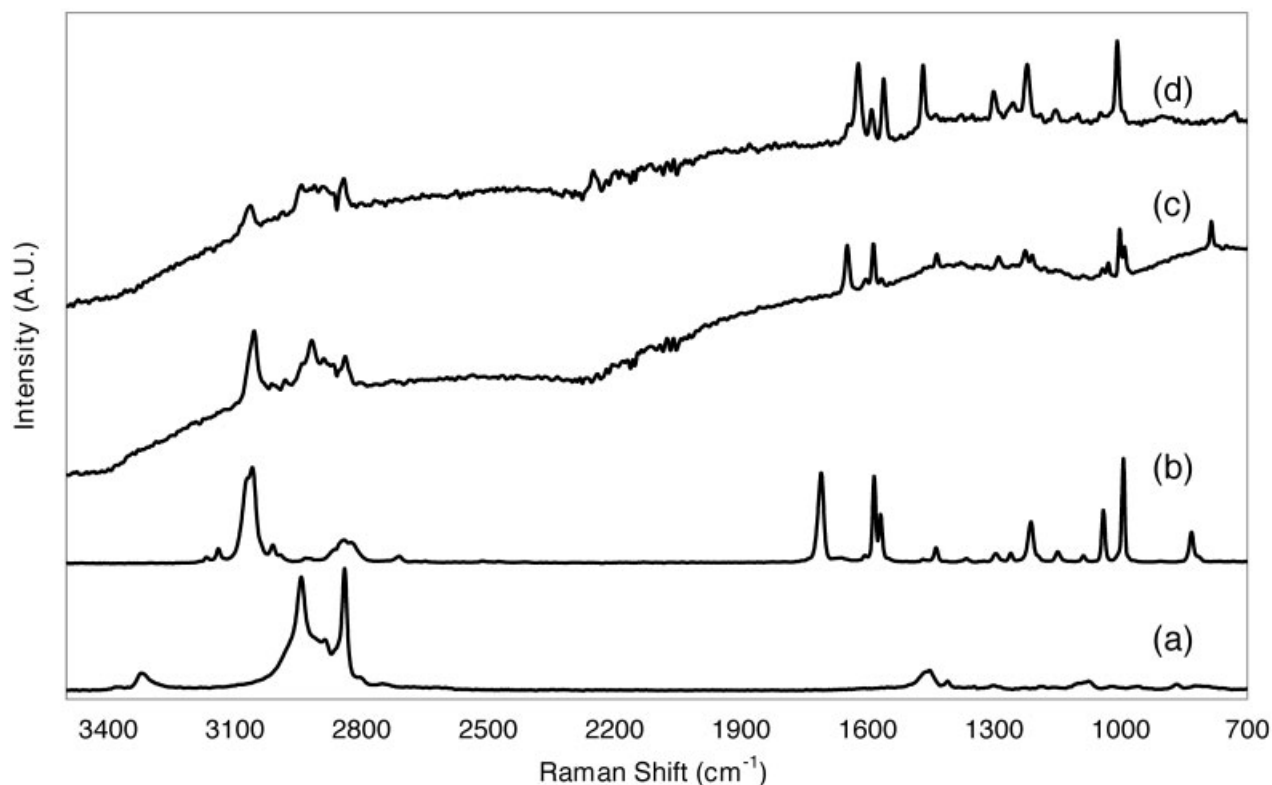


Figure 2. FT-Raman spectroscopy study of CuBr/PMITMS synthesis: (a) APS, (b) PCA, (c) PMITMS, and (d) CuBr/PMITMS.

CuBr were added to tetrahydrofuran (THF). The ν (imine), ν (pyridyl ring), and ν (in-plane CH) vibrations shift slightly to 1625, 1560, and 1007 cm^{-1} , respectively. This observation was attributed to the change in the chemical environment around the chelating nitrogen atoms due to CuBr coordination. These results are consistent with FT-Raman spectra of metal coordination complexes with bidentate chelating nitrogen ligands reported in the literature.⁵² However, the copper monocoordinated and biscoordinated PMI species could not be distinguished by FT-Raman spectroscopy. There also remain visible shoulders at 1650,

1585, and 993 cm^{-1} that can be assigned to the uncoordinated PMITMS ligand.

Silica Supports

The SBA15 materials were prepared according to a procedure previously described by Stucky and coworkers.^{49,50} For the 100-Å-pore material, TMB was used as a swelling agent to increase the pore size. The mesoporous silicates were characterized by nitrogen physisorption to determine the surface area and pore size of the pristine silica supports (Table 3). TGA approximated the total silica

Table 2. FT-Raman Results for Spectroscopic Studies of PMITMS

Entry	Compound	ν (N—H)	ν (Aliphatic CH)	ν (Aromatic CH)	ν (CHO)	ν (Pyridyl Ring)	ν (In-Plane CH)	ν (Imine)
1	APS	3313	2800–2900	—	—	—	—	—
2	PCA	—	2800–2900	3056	1708	1585	993	—
3	PMITMS	—	2800–2900	3056	—	1585	993	1650
4	CuBr/PMITMS	—	2800–2900	3056	—	1560	1007	1625

Table 3. Nitrogen Physisorption Results

Entry	Material	Pore Diameter (Å) ^a	BET Surface Area (SA) (m ² /g)	Silanol Concentration (mmol of OH/g of solid) ^b
1	SBA15(48)	48	701	~2.0
2	SBA15(100)	100	896	~2.0
3	Cab-O-Sil EH5	—	335	~2.7

^a Based on the BJH analysis of the adsorption branch of the isotherm.

^b Total silanol content as estimated by TGA.

nol concentration to be 2.0 mmol of OH/g of solid for 48- and 100-Å materials. X-ray powder diffraction was used to determine the order of the porosity and the overall structure of SBA15. The X-ray diffraction patterns (not shown) were consistent with a hexagonal pore structure.^{48–50}

Cab-O-Sil EH5 is a commercially available fumed, nonporous silica from Cabot. Multiparticle aggregates have a length of 0.2–0.3 μm (individual particles have nanosized features), a surface area of 335 m²/g, and 2.7 mmol of OH/g of solid according to nitrogen physisorption and TGA (this is consistent with the product data sheet⁵³).

Synthesis and Characterization of the Immobilized CuBr/PMI Complex on Silica

Synthesis

In M1, APTMS was covalently grafted onto pristine SBA15 (48-Å pores) to give a white powder containing about 1.36 mmol of amine/g of solid according to TGA; it was designated SBA15(48)-NH₂-M1. In the FT-Raman spectrum, the amine-functionalized SBA15 displayed a band at 3296 cm⁻¹ due to the primary amine [Fig. 3(a)]. Subsequently, PCA was added to the immobilized primary amine binding site, yielding the corresponding immobilized PMI ligand, to give a yellowish-white powder containing about 1.13 mmol of ligand/g of solid according to TGA; it was designated SBA15(48)-PMI-M1. Approximately 92% of the amines were converted into imines according to TGA. Figure 3(b) shows FT-Raman spectra of the SBA15(48)-PMI-M1 material. It shows the complete disappearance of the amine band (3296 cm⁻¹) and the appearance of bands at 3058, 1650, 1587, and 991 cm⁻¹, which correspond to ν(aromatic C—H), ν(imine), ν(pyridyl ring), and ν(in-plane CH), respectively. The FT-Raman spectrum was similar to that of the homogeneous PMITMS ligand [Fig. 2(c)], verifying the formation of the

intended ligand structure. The coordination of CuBr to the immobilized ligand was carried out through the treatment of SBA15(48)-PMI-M1 (2.00 g) with a slurry of CuBr (0.16 g, ligand/metal molar ratio = 2) in toluene at 110 °C. A dark reddish-brown solid was recovered and washed with copious amounts of dry toluene, hexanes, and dichloromethane. The solvent wash aided in the removal of much of the uncoordinated CuBr and physisorbed chemical species from the pores and support surface. This material was designated SBA15(48)-CuBr/PMI-M1. CHN and Cu analysis determined a surface loading of 1.07 mmol of ligand/g of catalyst and 0.48 mmol of Cu/g of catalyst, respectively. This corresponded to 89% of the PMI ligands complexed with CuBr. The percentage of PMI ligands complexed was calculated with the following equation:

$$\text{Complexed PMI (\%)} = \left\{ \frac{\text{(mmol of Cu} \times \text{g of catalyst}^{-1})}{[\text{(mmol of PMI ligand} \times \text{g of catalyst}^{-1})/2]} \right\} \times 100$$

A value of 100% PMI coordinated signifies that the number of Cu atoms is consistent with coordination to two immobilized PMI ligands. Deviations from 100% mean that uncoordinated PMI ligands must exist (<100%), Cu monocoordinated PMI ligands likely exist (100 > X > 200%), or Cu adsorbed to the silica surface with no organic ligand likely exists (>200%). This quantity is only a measure of the metallation efficiency and should not be used as the only indication of what surface species exist on the silica surface. FT-Raman spectroscopy showed vibrational shifts, after metallation, of the ν(imine), ν(pyridyl ring), and ν(in-plane C—H) signals to 1625, 1562, and 1007 cm⁻¹, respectively [Fig. 3(c)]. This was consistent with the FT-Raman spectrum of CuBr/PMITMS in Figure 2(d), verifying Cu coordina-

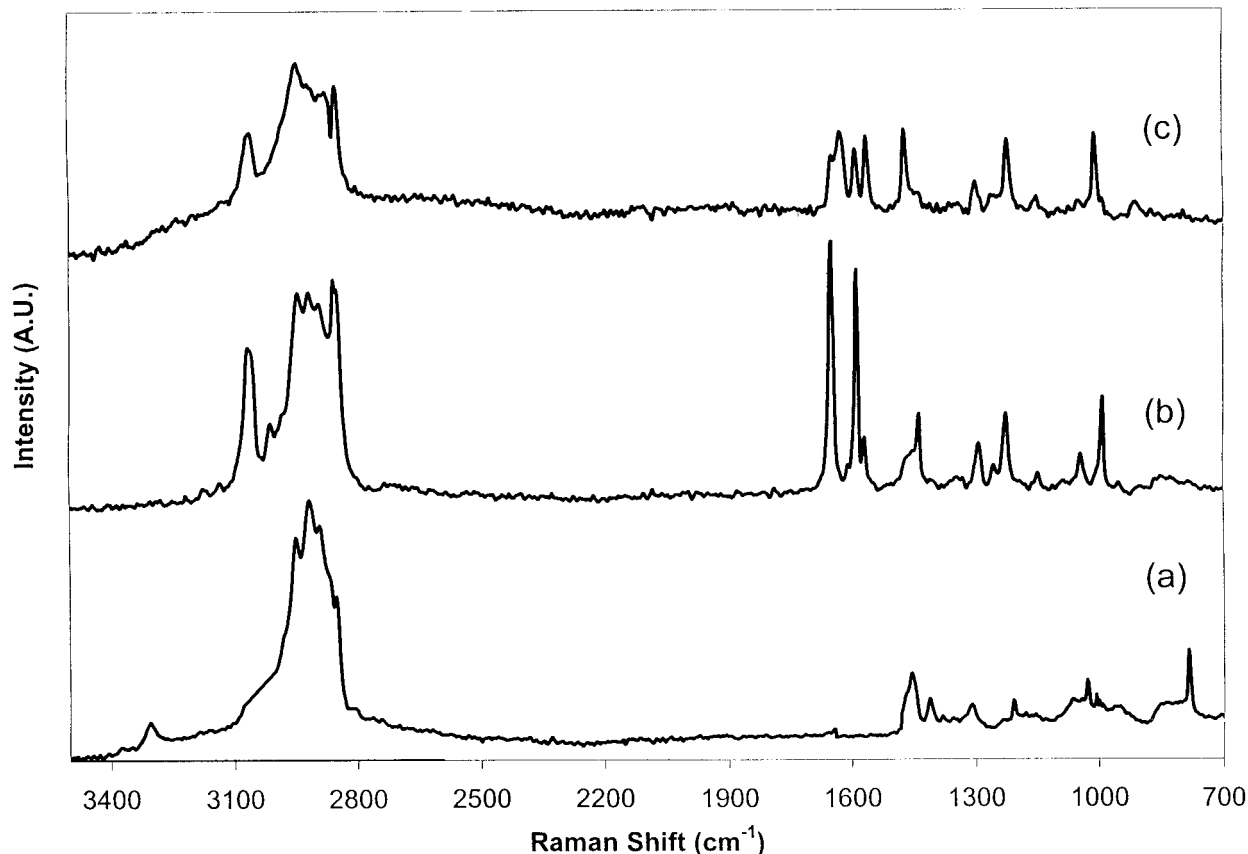


Figure 3. FT-Raman spectroscopy study of the multistep-grafting approach to SBA15(48): (a) SBA15(48)-NH₂-M1, (b) SBA15(48)-PMI-M1, and (c) SBA15(48)-CuBr/PMI-M1.

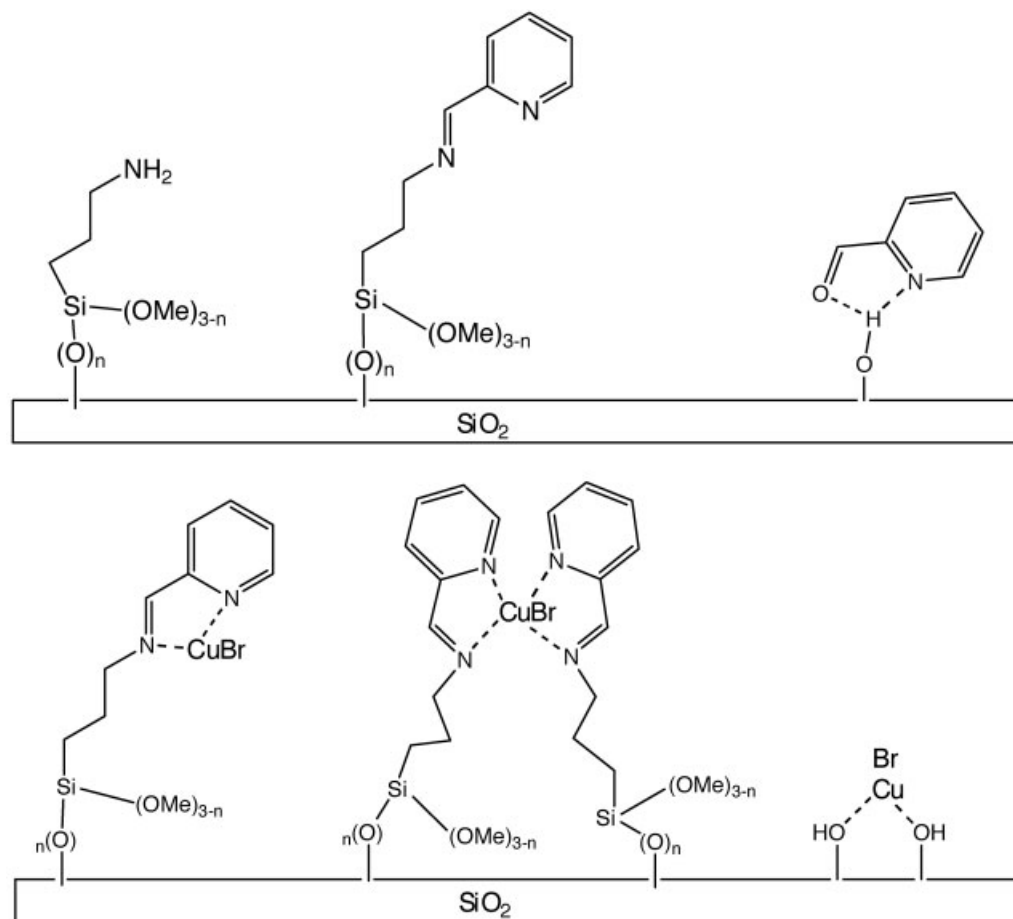
tion by the ligand. However, there remains a visible shoulder at 1650 cm⁻¹, which has been attributed to the uncoordinated ligand. Again, the distinction between copper monocoordinated and biscoordinated PMI ligands could not be assigned, for reasons already mentioned.

The use of an immobilizable PMITMS ligand in M2-M4 eliminates the inherent uncertainty in M1 of how much ligand is loaded on the silica surface. The use of PMITMS can also reduce the number of different organic functionalities that can exist on the surface to complete PMI ligands (no adsorbed aldehyde or free amine if the preformed ligand remains intact), but it does not eliminate the many different ways in which the PMI ligand can interact with the surface and the metal halide. Scheme 4 shows some of the numerous *possible* surface functionalities on silica when the multistep-grafting approach is used.

M2, the two-step approach, first involved covalently grafting the PMITMS ligand onto SBA15 similarly to APTMS, yielding a yellowish-white

powder containing about 1.13 mmol of ligand/g of solid; it was designated SBA15(48)-PMI-M2. The FT-Raman spectra for this material showed signals identical to those for SBA15(48)-PMI-M1. Figure 4 shows the solid-state ¹³C CP-MAS NMR results for the direct immobilization of the PMITMS ligand. The lower spectrum is the solution ¹³C NMR spectrum of PMITMS [Fig. 4(a)]. The ¹³C CP-MAS NMR spectrum of SBA15(48)-PMI-M2 [Fig. 4(b)] possesses the same signals as the homogeneous form, but it is much broader because the PMI ligands are now immobilized. The signal at 8.7 ppm corresponds to the -CH₂Si- carbon, indicating that the PMI ligands were covalently anchored to the silica surface. The weak band in the region between 192 and 190 ppm was determined to be the spinning sideband of the 122.8 and 120.2 ppm signals.

The metallation of SBA15(48)-PMI-M2 was performed in a similar manner to M1, yielding a dark reddish-brown powder consisting of about 1.09 mmol of ligand/g of catalyst, 0.51 mmol of



Scheme 4

Cu/g of catalyst, and 95% PMI complexed; it was designated SBA15(48)-CuBr/PMI-M2. The FT-Raman spectrum of SBA15(48)-CuBr/PMI-M2 was again comparable to that of SBA15(48)-CuBr/PMI-M1, but the shoulder at 1650 cm^{-1} was not as pronounced. With the PMITMS ligand, the incomplete conversion of the amine species and the reaction of the PCA ligand precursor with the silica surface may be completely avoided. However, the method does not eliminate CuBr from adsorbing to the surface silanols.

The one-pot and preassembled-complex approaches (M3 and M4, respectively) were devised to improve the metallation step of the supported catalyst. It was envisioned that the immobilizable ligand would self-assemble with the metal, ideally with a ligand/metal ratio of 2, and then covalently attach to the silica surface. M3 involved adding all the reagents and support in one pot, whereas M4 involved preassembling the metal/ligand complex *in situ* and then adding the support. Both methods yielded dark reddish-brown

powders that were washed extensively with solvents to remove free PMITMS ligand, CuBr/PMITMS complex, and CuBr that remained in the pores and on the surface. Solids prepared in this way were designated SBA15(48)-CuBr/PMI-M3 and SBA15(48)-CuBr/PMI-M4, respectively. CHN and Cu analyses of the solids indicated loadings of 1.02 mmol of ligand/g of catalyst, 0.42 mmol of Cu/g of catalyst, and 83% PMI complexed (M3) and 1.07 mmol of ligand/g of catalyst, 0.48 mmol of Cu/g of catalyst, and 89% ligands complexed (M4). FT-Raman spectra of both catalysts were similar to the metallated spectra for M1 and M2, with a shoulder still appearing in the M3 spectrum and little or no shoulder appearing in the M4 spectrum. A comparison of the FT-Raman spectra of CuBr/PMI complexes immobilized on SBA15(48) (M1-M4) is shown in Figure 5.

The syntheses of the CuBr/PMI complex immobilized on SBA15 (100-Å pores) and Cab-O-Sil EH5 for each method were performed in a manner

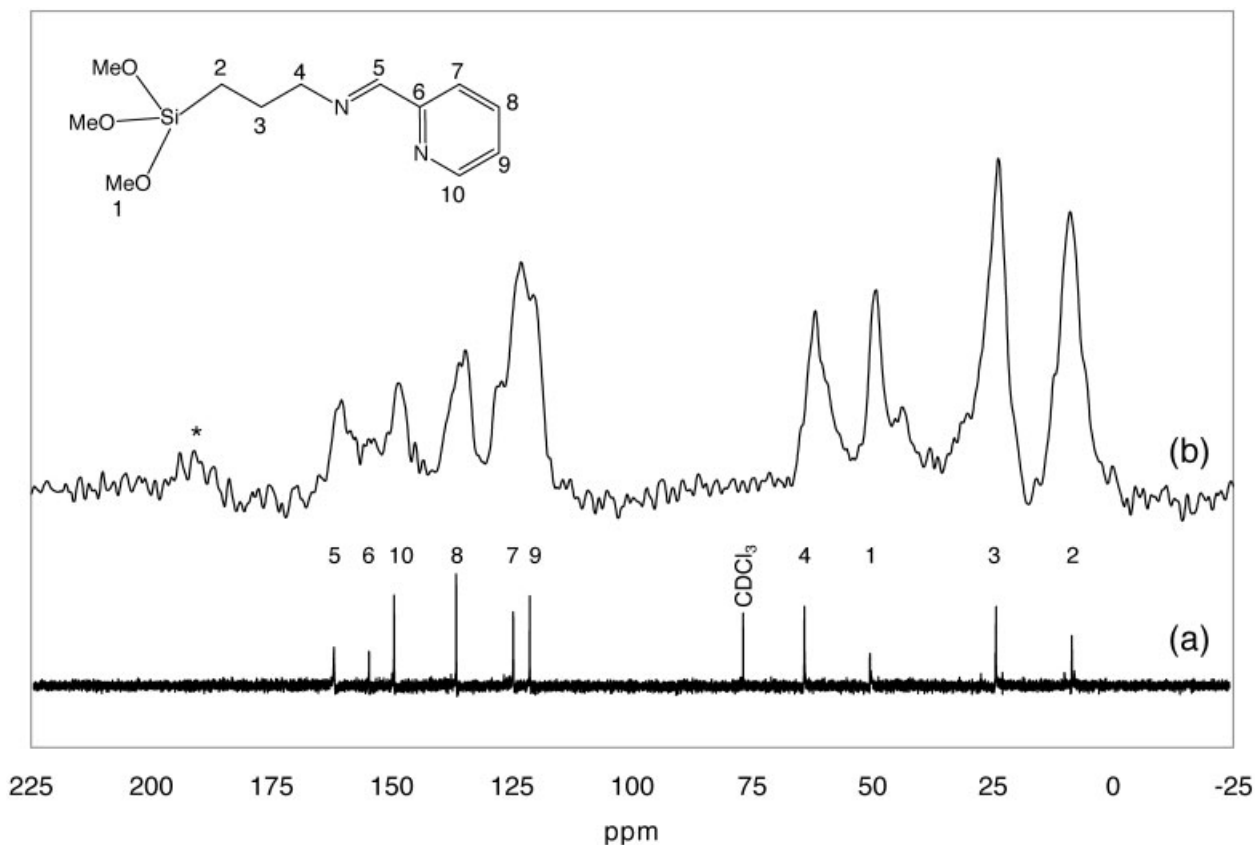


Figure 4. (a) Solution and (b) solid-state CP-MAS total sideband suppression (TOSS) NMR spectra of PMITMS in CDCl_3 and SBA15(48)-PMI-M2, respectively. The asterisk indicates a spinning sideband for the signal centered between 122 and 120 ppm.

similar to that described previously. Table 4 summarizes the complete TGA and EA results. These catalysts were synthesized on various silica supports to determine how the silica support structure changed the polymerization performance.

Surface Structure and Composition

Table 4 summarizes the results from TGA and EA. The ligand loadings were calculated on the basis of two —OMe units reacting to the silica surface. This was confirmed by solid-state ^{29}Si magic-angle-spinning (MAS) and CP-MAS NMR results (the CP-MAS spectrum is shown in Fig. 6). From the ^{29}Si spectrum, three signals at -50.2 , -57.6 , and -64.4 ppm were identified as T^1 , T^2 , and T^3 sites, respectively.⁵⁴ The signals correspond to one, two, and three —OMe units reacting to the silica surface. The T^2 signal was the predominant signal in both the MAS and CP-MAS spectra, and this suggested that most of the PMI ligands were anchored by two —Si—O— bonds to

the surface, but a distribution of one, two, and three surface-anchored PMI ligands existed. The TGA ligand loadings were determined by the organic loss between 200 and 500 °C. The EA ligand loadings were calculated on the basis of the total carbon content by CHN analysis. The TGA and EA ligand loadings agreed well, and the differences were within reasonable experimental error between the two techniques. The ligand loadings were approximately 1.0 mmol of PMI/g of catalyst for all the materials.

On the basis of the BET surface area of the silica supports and the ligand loadings determined by EA, on average the number of PMI ligands per square nanometer for SBA15(48), SBA15(100), and Cab-O-Sil EH5 was 1.20, 1.15, and 2.60 PMI ligands/ nm^2 , respectively. This quantity is an average measure of how far apart the ligands are spaced on the surface. These values are important, as the proximity of ligands to one another will influence the biscoordination ability of the immobilized complexes. Statisti-

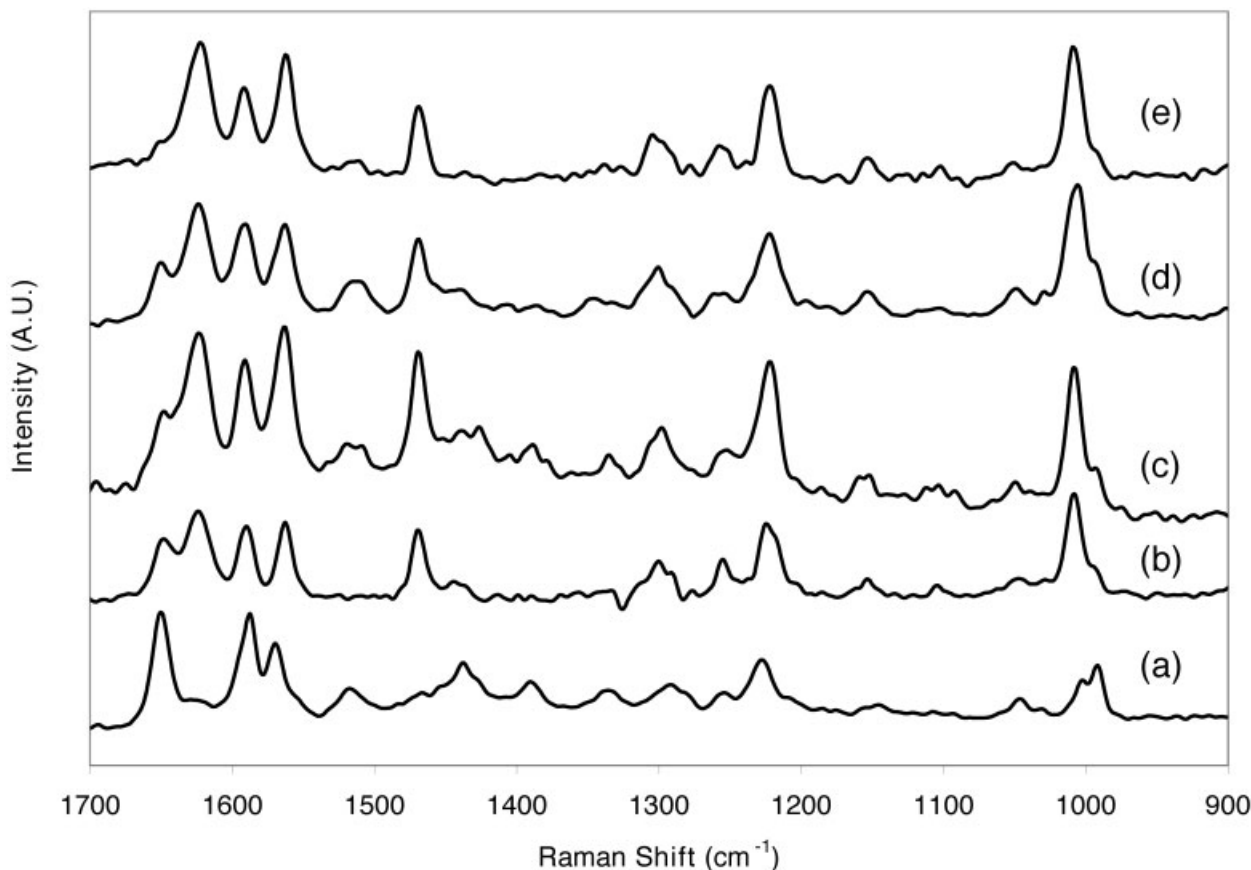


Figure 5. FT-Raman spectra of SBA15(48) obtained with different synthetic methods: (a) SBA15(48)–PMI-M2, (b) SBA15(48)–CuBr/PMI-M1, (c) SBA15(48)–CuBr/PMI-M2, (d) SBA15(48)–CuBr/PMI-M3, and (e) SBA15(48)–CuBr/PMI-M4.

cally, PMI ligands supported on Cab-O-Sil EH5 have a greater opportunity to have two PMI ligands coordinated to one CuBr because they are closer in proximity to one another on average. This advantage may be less important in catalysts prepared with M4, as a preformed bis-complex is formed before immobilization in this case.

Spectroscopic Studies of CuBr Coordination

Each subsequent method was designed to improve the metallation of the catalyst and to investigate the catalyst performance. Figure 5 shows a comparison of the FT-Raman spectra for M1–M4 on 48-Å SBA15 in the range of 900–1700 cm^{-1} . Figure 5(a) shows SBA15(48)–PMI-M2, an uncoordinated covalently bound PMI ligand. The signals of interest are ν (imine), ν (pyridyl ring), and ν (in-plane ring) at 1650, 1585, and 991 cm^{-1} , respectively. When CuBr was coordinated to the

immobilized PMI ligand, the ν (imine), ν (pyridyl ring), and ν (in-plane ring) signals shifted to 1625, 1560, and 1007 cm^{-1} , respectively. The efficiency of the metallation can be qualitatively interpreted from the shoulder remaining at 1650 cm^{-1} . The increasing metallation efficiency of CuBr/PMI complexes immobilized on SBA15(48) can be described as follows: $M1 < M3 \leq M2 < M4$ (interpreted from Fig. 5). This observation could not be distinguished by TGA and EA because these techniques only give the total elemental or organic loading. If the metallation efficiency was based on EA alone, it would be described as follows: $M3 < M2 < M4 < M1$. This ranking of the efficiency of coordination may be the immobilized CuBr/PMI complexes is inaccurate, as indicated by the FT-Raman spectra. Although the percentage of PMI complexed suggested more than 80% of the PMI ligands were coordinated for SBA15(48) materials, the intensity of the shoulder at 1650 cm^{-1} for M1, M2, and M3 indicates the percentage of

Table 4. TGA and EA of Silica-Supported CuBr/PMI Complexes

Entry	Materials	TGA PMI Loading (mmol/g of catalyst) ^a	EA PMI Loading (mmol/g of catalyst) ^b	EA Cu Loading (mmol/g of catalyst) ^c	% Loaded (TGA, EA) ^d	Ligand Density (PMI/nm ²)
1	SBA(48)-CuBr/PMI-M1	0.99	1.07	0.48	97, 89	1.23
2	SBA(48)-CuBr/PMI-M2	1.13	1.09	0.51	91, 95	1.23
3	SBA(48)-CuBr/PMI-M3	1.13	1.02	0.42	75, 83	1.14
4	SBA(48)-CuBr/PMI-M4	1.03	1.07	0.48	93, 89	1.22
5	SBA(100)-CuBr/PMI-M1	1.30	1.18	0.62	96, 106	1.16
6	SBA(100)-CuBr/PMI-M2	1.08	1.19	0.48	90, 81	1.08
7	SBA(100)-CuBr/PMI-M3	1.20	1.30	0.56	93, 86	1.23
8	SBA(100)-CuBr/PMI-M4	1.35	1.21	0.49	72, 81	1.12
9	Cab-O-Sil-CuBr/PMI-M1	0.94	0.88	0.43	91, 98	1.98
10	Cab-O-Sil-CuBr/PMI-M2	0.87	0.98	0.37	84, 75	2.24
11	Cab-O-Sil-CuBr/PMI-M3	1.14	1.27	0.71	125, 112	3.30
12	Cab-O-Sil-CuBr/PMI-M4	1.12	1.19	0.50	89, 84	2.88

^a Ligand loading based on TGA of the organic mass loss (%) between 200 and 500 °C.

^b Ligand loading based on EA of the carbon content (%).

^c Copper loading based on EA of the copper content (%).

^d PMI ligand complexed (%) based on the ligand/metal ratio (2).

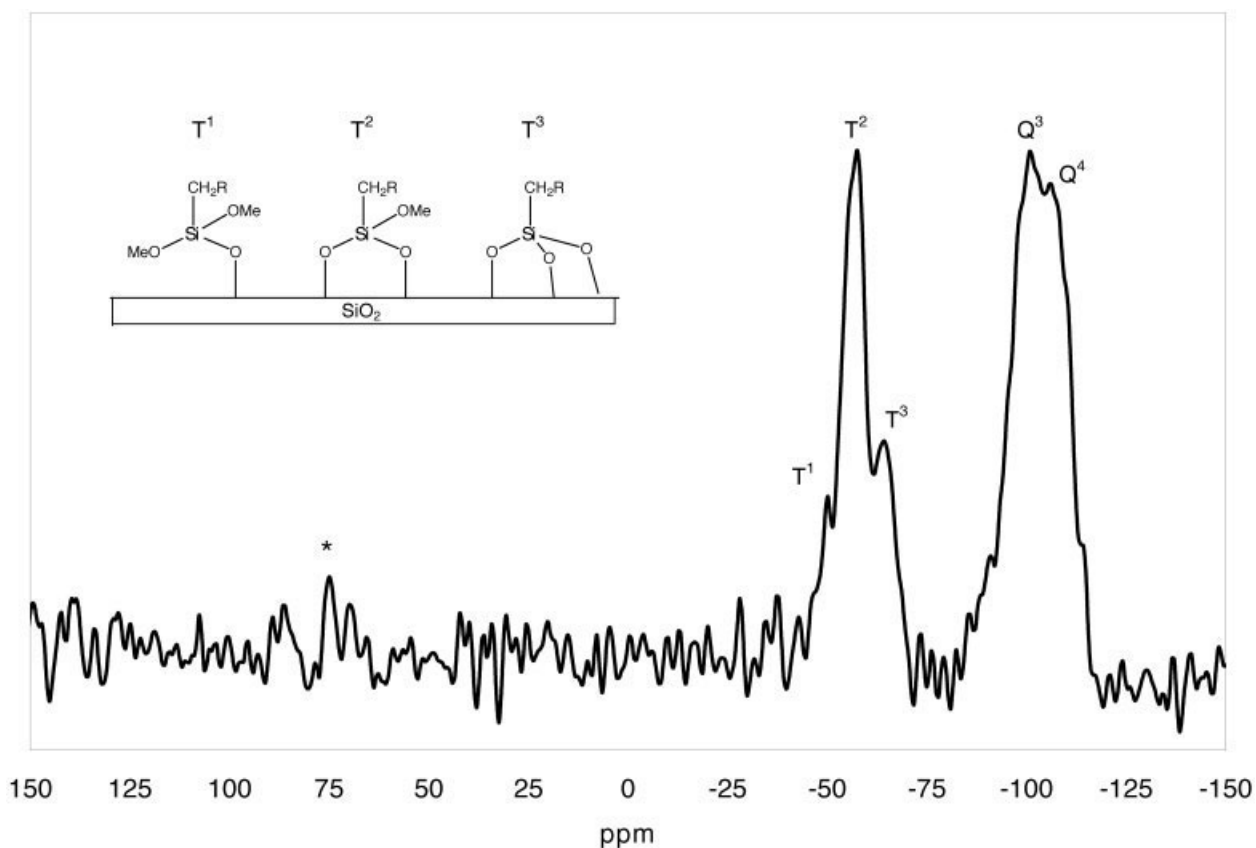


Figure 6. Solid-state ²⁹Si CP-MAS NMR spectrum of SBA15-PMI-M2. The asterisk indicates a spinning sideband for the signal centered at -57 ppm.

the uncoordinated ligand could be higher than 20%. To rationalize the differences in the coordination inferred from the EA and FT-Raman data, we can speculate that free CuBr may be adsorbed to the silica surface via a Si—OH—CuBr interaction, resulting in inflated percentages of PMI complexed, especially for M1–M3. In a control experiment, it was found that after CuBr was mixed in a solution of toluene and bare silica, EA of the recovered silica powder revealed a large concentration of Cu (3.6 mmol of Cu/g of SiO₂), even after extensive washing with toluene, hexane, dichloromethane, and THF. Therefore, organic-ligand-free sections of the silica supports can effectively adsorb free CuBr if the uncomplexed metal salt is in contact with the supports.

On a molecular level, there are five competing processes involving the immobilization of the CuBr/PMI complex: (1) the rate of CuBr coordinating to the surface-immobilized PMI ligand, (2) the rate of bare CuBr adsorbing to silica, (3) the rate of PMITMS reacting to surface, (4) the rate of mono CuBr/PMITMS reacting to the surface, and (5) the rate of bis CuBr/PMITMS reacting to the surface. M1 and M2 involve the first two processes; because M1 possesses the less defined immobilized PMI ligand, the metallation is worse. M3 potentially involves all five processes. In M4, the CuBr molecules are coordinated to the free PMITMS ligand before the addition of the silica source, and so rates 4 and 5 are expected to be of primary importance. Because the metallation occurs in a homogeneous solution in M4, it is more likely to produce surface structures that are akin to what is believed to be the homogeneous catalyst than in M1–M3.

CONCLUSIONS

A number of methodologies for the immobilization of CuBr/PMI ATRP complexes on silica supports have been evaluated. Four different methods were used on three structurally different silica supports. The catalysts were characterized by TGA, EA, and FT-Raman spectroscopy. Solid-state ¹³C and ²⁹Si CP-MAS NMR results indicated that the intended PMI ligands were immobilized on the silica surface and predominantly consisted of intact PMI ligands anchored by two —Si—O— bonds. The PMI ligand loadings agreed well within experimental error between TGA and EA. The results suggested that more than 80% of the ligands were coordinated to CuBr for all the

synthetic methods. This suggested that some uncoordinated PMI ligands existed on the silica surface. However, the intensity of the shoulder at 1650 cm⁻¹, attributed to the uncomplexed ligand, in the FT-Raman spectrum indicated that potentially fewer PMI ligands were coordinated for M1, M2, and M3. This suggested that perhaps CuBr adsorbed to the silica surface in samples made with these methods. The metallation efficiency increased as follows: M1 < M3 ≤ M2 < M4 (qualitatively determined by FT-Raman spectroscopy from the residual shoulder at 1650 cm⁻¹). This differed from the overall metal loading of the solids determined by EA: M3 < M2 < M4 < M1. This ranking determined by EA included physisorbed, organic-ligand-free CuBr species that appeared to be present in catalysts made by M1–M3. M4, the approach using a preassembled complex, appeared to result in a more structurally homogeneous immobilized ATRP complex. The immobilized CuBr/PMI complexes will be tested for the polymerization of MMA. The overall performance of these catalysts will be compared against each synthetic approach and as a function of the silica support structure in the second part of this series.⁴⁶

The National Science Foundation is gratefully acknowledged for its partial support of this work (CTS-0210460). C. W. Jones thanks the Shell Oil Company Foundation and Oak Ridge Associated Universities for their partial support of this work through a Faculty Career Initiation Award and a Ralph Powe Junior Faculty Award, respectively. The authors thank Angus Wilkinson for the use of the X-ray diffractometer and Johannes Liesen for his advice on solid-state NMR experiments.

REFERENCES AND NOTES

1. Wang, J.; Matyjaszewski, K. *J Am Chem Soc* 1995, 117, 5614–5615.
2. Wang, J.; Matyjaszewski, K. *Macromolecules* 1995, 28, 7572–7573.
3. Wang, J.; Matyjaszewski, K. *Macromolecules* 1995, 28, 7901–7910.
4. Kato, M.; Kamigaito, M.; Sawamoto, M.; Higashimura, T. *Macromolecules* 1995, 28, 1721–1723.
5. Wang, J.; Matyjaszewski, K. *Chem Rev* 2001, 101, 2921–2990.
6. Huang, X.; Wirth, M. J. *Anal Chem* 1997, 69, 4577–4580.
7. Kim, J.-B.; Huang, W.; Miller, M. D.; Baker, G. L.; Bruening, M. L. *J Polym Sci Part A: Polym Chem* 2003, 41, 386–394.

8. Matyjaszewski, K.; Qiu, J.; Tsarevsky, N. V.; Charleux, B. *J Polym Sci Part A: Polym Chem* 2000, 38, 4724–4734.
9. Cunningham, M. F. *Prog Polym Sci* 2002, 27, 1039–1067.
10. Qiu, J.; Charleux, B.; Matyjaszewski, K. *Prog Polym Sci* 2001, 26, 2083–2134.
11. Li, M.; Matyjaszewski, K. *J Polym Sci Part A: Polym Chem* 2003, 41, 3606–3614.
12. Hoogenboom, R.; Schubert, U. S. *J Polym Sci Part A: Polym Chem* 2003, 41, 2425–2434.
13. It has been demonstrated that good rates and control can be achieved with substantially smaller amounts of metal complexes in homogeneous systems; see Queffelec, J.; Gaynor, S. G.; Matyjaszewski, K. *Macromolecules* 2000, 33, 8629–8639.
14. Matyjaszewski, K.; Pintauer, T.; Gaynor, S. *Macromolecules* 2000, 33, 1476–1478.
15. Haddleton, D. M.; Jackson, S. G.; Bon, S. A. F. *J Am Chem Soc* 2000, 122, 1542–1543.
16. Angot, S.; Ayres, N.; Bon, S. A. F.; Haddleton, D. M. *Macromolecules* 2001, 34, 768–774.
17. Biedron, T.; Kubisa, P. *Macromol Rapid Commun* 2001, 22, 1237–1242.
18. Sarbu, T.; Matyjaszewski, K. *Macromol Chem Phys* 2001, 202, 3379–3391.
19. Carmichael, A. J.; Haddleton, D. M.; Bon, S. A. F.; Seddon, K. R. *Chem Commun* 2000, 1237–1238.
20. Honigfort, M. E.; Brittain, W. J.; Bosanac, T.; Wilcos, C. S. *Macromolecules* 2002, 35, 4849–4851.
21. Kickelbick, G.; Paik, H. J.; Matyjaszewski, K. *Macromolecules* 1999, 32, 2941–2947.
22. Hong, S. C.; Paik, H. J.; Matyjaszewski, K. *Macromolecules* 2001, 34, 5099–5102.
23. Hong, S. C.; Matyjaszewski, K. *Macromolecules* 2002, 35, 7592–7605.
24. Hong, S. C.; Neugebauer, D.; Inoue, Y.; Lutz, J. F.; Matyjaszewski, K. *Macromolecules* 2003, 36, 27–35.
25. Hong, S. C.; Lutz, J. F.; Inoue, Y.; Strissel, C.; Nuyken, O.; Matyjaszewski, K. *Macromolecules* 2003, 36, 1075–1082.
26. Haddleton, D. M.; Kukulj, D.; Radigue, A. P. *Chem Commun* 1999, 99–100.
27. Haddleton, D. M.; Duncalf, D. J.; Kukulj, D.; Radigue, A. P. *Macromolecules* 1999, 32, 4769–4775.
28. Liou, S.; Rademacher, J. T.; Malaba, D.; Pallack, M. E.; Brittain, W. J. *Macromolecules* 2000, 33, 4295–4296.
29. Honigfort, M. E.; Brittain, W. J. *Macromolecules* 2003, 36, 3111–3114.
30. Shen, Y.; Zhu, S.; Zeng, F.; Pelton, R. *Macromol Chem Phys* 2001, 201, 1387–1394.
31. Shen, Y.; Zhu, S.; Zeng, F.; Pelton, R. *Macromolecules* 2000, 33, 5427–5431.
32. Shen, Y.; Zhu, S.; Pelton, R. *Macromolecules* 2001, 34, 3182–3185.
33. Shen, Y.; Zhu, S.; Zeng, F.; Pelton, R. *J Polym Sci Part A: Polym Chem* 2001, 39, 1051–1059.
34. Shen, Y.; Zhu, S.; Pelton, R. *Macromolecules* 2001, 34, 5812–5818.
35. Shen, Y.; Zhu, S. *Macromolecules* 2001, 34, 8603–8609.
36. Shen, Y.; Zhu, S.; Pelton, R. *Macromol Rapid Commun* 2000, 21, 956–959.
37. Opstal, T.; Melis, K.; Verpoort, F. *Catal Lett* 2001, 74, 155–159.
38. Pintauer, T.; Qiu, J.; Kickelbick, G.; Matyjaszewski, K. *Inorg Chem* 2001, 40, 2818–2824.
39. Kickelbick, G.; Pintauer, T.; Matyjaszewski, K. *New J Chem* 2002, 26, 462–468.
40. Haddleton, D. M.; Duncalf, D. J.; Kukulj, D.; Crossman, M. C.; Jackson, S. G.; Bon, S. A. F.; Clark, A. J.; Shooter, A. J. *Eur J Inorg Chem* 1998, 11, 1799–1806.
41. Haddleton, D. M.; Jasieczek, C. B.; Hannon, M. J.; Shooter, A. J. *Macromolecules* 1997, 30, 2190–2193.
42. Dai, S.; Burleigh, M. C.; Ju, Y. H.; Gao, H. J.; Lin, J. S.; Pennycook, S. J.; Barnes, C. E.; Xue, Z. L. *J Am Chem Soc* 2000, 122, 992–993.
43. Dai, S.; Burleigh, M. C.; Shin, Y.; Morrow, C. C.; Barnes, C. E.; Xue, Z. *Angew Chem Int Ed* 1999, 38, 1235–1239.
44. Zhang, Z.; Dai, S.; Hunt, R. D.; Wei, Y.; Qiu, S. *Adv Mater* 2001, 13, 493–496.
45. For an example of PMI ligands in solution polymerizations, see Zhang, H. Q.; Van Der Linde, R. *J Polym Sci Part A: Polym Chem* 2002, 40, 3549–3561.
46. Nguyen, J. V.; Jones, C. W. *J Polym Sci Part A: Polym Chem*, 2004, in press.
47. Pangborn, A. M.; Giardello, M. A.; Grubbs, R. H.; Rosen, R. K.; Timmers, F. J. *Organometallics* 1996, 15, 1518–1520.
48. Kruk, M.; Jaroniec, M. *Chem Mater* 2000, 12, 1961–1968.
49. Zhao, D.; Feng, J.; Huo, Q.; Melosh, N.; Frederickson, G. H.; Chmelka, B. F.; Stucky, G. D. *Science* 1998, 279, 548–552.
50. Zhao, D.; Huo, Q.; Feng, J.; Chmelka, B. F.; Stucky, G. D. *J Am Chem Soc* 1998, 120, 6024–6036.
51. Baranska, H.; Labudzinska, A.; Terpinski, J. *Laser Raman Spectrometry*; Wiley: New York, 1987.
52. Nunes, C. D.; Pillinger, M.; Valente, A. A.; Goncalves, I. S.; Rocha, J.; Ferreira, P.; Kuhn, F. E. *Eur J Inorg Chem* 2002, 1100–1107.
53. Product Data Sheet for Untreated Fumed Silica Cab-O-Sil EH5; Cabot Corp.; Tuscola, IL, USA (<http://www.cabot-corp.com>), 2002.
54. Sindorf, D. W.; Maciel, G. E. *J Am Chem Soc* 1983, 105, 3767–3776.